Biointerface Research in Applied Chemistry
Platinum Open Access Journal (ISSN: 2069-5837)

Article
Volume 11, Issue 3, 2021, 10265 - 10277
https://doi.org/10.33263/BRIAC113.1026510277

Activated Carbon from Rice Husk Biochar with High Surface Area

Enelise Scapin [1], Gabriela Pereira da Silva Maciel [2], Allan dos Santos Polidoro [1], Eliane Lazzari [1], Edilson Valmir Benvenutti [1], Tiago Falcade [1], Rosângela Assis Jacques [1,3,*]

[1] Instituto de Química, Universidade Federal do Rio Grande do Sul (UFRGS), Porto Alegre, RS, Brasil
[2] Departamento Interdisciplinar, UFRGS- Campus Litoral Norte, Tramandaí, RS, Brasil
[3] Instituto Nacional de Ciência e Tecnologia em Energia e Ambiente, INCT-EA, Salvador, Bahia, Brasil
* Correspondence: rosangela.j@iq.ufrgs.br;

Scopus Author ID 11739487200

Received: 1.09.2020; Revised: 9.10.2020; Accepted: 11.10.2020; Published: 14.10.2020

Abstract: Activated carbons derived from rice husk pyrolysis (biochar) were prepared by chemical activation at different biochar/K_2CO_3 proportions in order to assess its capacity as adsorbent. The activated material was characterized by X-ray diffraction (DRX), Raman spectroscopy, scanning electron microscopy (SEM), the Brunauer, Emmet, and Teller (BET) method. The Barret, Joyner, and Halenda (BJH) method and functional density theory (DFT), presenting interesting texture properties, such as high surface area (BET 1850 m^2 g^{-1}) and microporosity, which allow its use as a sorbent phase in solid-phase extraction (SPE) of the main constituents of the aqueous pyrolysis phase. It was demonstrated that the activated carbon (RH-AC) adsorbs different compounds present in from rice husk pyrolysis wastewater through quantitative analysis by high-performance liquid chromatography with a diode-array detector (HPLC-DAD), presenting good linearity (R2 > 0.996) at 280 nm.

Keywords: activated carbon; rice husk; adsorption; biochar; SPE; HPLC-DAD

1. Introduction

A growing number of studies have explored methods for transforming agro-industrial waste into high value-added products [1–8]. Among these waste sources, rice husk (RH) is a good alternative because it provides large amounts of silica and organic matter [9]. Brazil produces approximately 10 million tons of rice per year, and the state of Rio Grande do Sul is the largest domestic producer, accounting for 66% of the national production [10,11]. Among the by-products, the husk accounts for the largest volume obtained during the rice processing, and furthermore, it accounts for an average of 25% of the final weight [12,13]. Rice husk disposal has become a serious environmental problem due to its slow decomposition, high concentration of organic compounds, and the great amount generated annually [14].

Pyrolysis could be used to reduce this waste and to produce high value-added materials. This process involves the thermal conversion of biomass using elevated temperatures in inert atmospheres (usually between 400 and 1000 °C) into gaseous, liquid products (bio-oil and aqueous phase) and solid products (biochar and ash) [1–8].

The aqueous phase is generated due to the water content of the raw material and dehydration reactions. In some cases, the aqueous phase is more than 70% of the biomass by weight [15,16]. The aqueous phase typically consists of polar organic compounds, such as furaldehydes, phenols, and ketones. As such, additional treatments are required to prevent these

complex chemicals from contaminating the environment [17]. The use of SPE for extracting and isolating organic compounds from aqueous phases plays an important role in the characterization of these compounds [18].

SPE is widely used in various industries, including environmental, petrochemical, pharmaceutical, biological, food, and forensic chemistry [19,20]. In order for a bio-char obtained from the pyrolysis of the rice husk to be considered a solid with adsorbent potential in SPE, it needs to undergo a chemical activation process, making it highly porous and with relatively increased surface area [21–26].

Chemical activation processes using NaOH/KOH [27–31], H_3PO_4 [32], or $ZnCl_2$ [30,33] have been widely used to dehydrate, unblock the pores and obtain an AC with significant porosity for adsorption. The use of an activating agent more sustainable and easily removed by water, such as K_2CO_3, has also been extensively exploited for producing a high surface area AC [21,27,34–42].

Therefore, in view of the excellent results generated in the chemical activation of the bio-char obtained from the rice husk pyrolysis, an evaluation of its application as an SPE phase was carried out in order to remove environmentally harmful organic compounds from the bio-oil aqueous phase. Furthermore, recovery of the aqueous phase aldehyde compounds, which has a great interest in the industry, has been evaluated by HPLC-DAD [43–49].

2. Materials and Methods

2.1. Samples and standards.

Rice husk was obtained from local industry in the Rio Grande do Sul state (Brazil). All solvents and reference standards (hydroquinone, 1,2-dihydroxybenzene (catechol), 5-hydroxymethylfurfural, 1,3-benzenediol (resorcinol), 3-methyl-1,2-cyclopentadione, 4-hydroxybenzaldehyde, 2-methoxyphenol (guaiacol), 2,6-dimethoxyphenol (syringol), 5-methyl furfural, phenol, furfural and Homovanillyl alcohol were purchased from Sigma–Aldrich (St. Louis, MO, USA) and were of high purity grade. Water was purified using a Milli-Q system (Millipore, Bedford, MA, USA). A methanol grade-HPLC was purchased from Tedia (Ohio, USA), and the Milli-Q water was generated using a Millipore System (Darmstadt, Germany) with 18 MΩ·cm conductivity.

2.2. Pyrolysis.

Prior to pyrolysis, samples of rice husk were dried in an oven at 60 °C for 1 hour. Pyrolysis experiments were carried out under a nitrogen atmosphere in a tubular fixed-bed oven with a quartz reactor, as described by Moraes *et al.* [3]. Briefly, 6 g of entire dried rice husk was employed in each pyrolysis run. Several temperatures between 430 ºC and 620 ºC were tested in order to obtain a higher amount of solid product. Then, the reactor was heated to the desired temperature of 480 °C at 100 °C min^{-1} and maintained at this temperature for 15 min under a constant nitrogen flow of 38.5 mL min^{-1}. At the end of the pyrolysis process, the solid product was designated as RH-Biochar. The yield calculation was performed using Equation 1. For this calculation, the difference between the empty flask and the flask containing the biochar was used.

Equation 1: $$Yield\ (\%) = \frac{\text{Biochar weight(g)}}{\text{Biomass weight(g)}} \times 100$$

Crude bio-oil was separated into an organic phase and an aqueous phase by simple decantation. The aqueous phase was analyzed by HPLC-DAD. For the HPLC analysis, the aqueous phase samples were diluted in Milli-Q water 1:40 (v/v) and filtered through a PTFE membrane of 0.20 µM pore size.

2.3. Chemical activation.

The chemical activation of the rice husk biochar using a K_2CO_3 activating agent was performed in a horizontal oven containing a quartz tube under N_2 flow (0.6 L min^{-1}). The temperature was increased (25 °C min^{-1}) to the activation temperature (800 °C or 900 °C) and maintained for 2 h. The temperature was set and controlled using a K-type thermocouple and a digital controller. After cooling under N_2 flow, the sample was washed with distilled water to pH 7 and dried at 100 °C. To prepare the activated carbon, biochar was mixed with K_2CO_3 at 1:1, 1:2, and 1:3 weight ratios of biochar/K_2CO_3. The activated materials were assigned as RH-AC/Biochar:K_2CO_3 (w/w)/T (°C).

2.4. Characterization of activated carbon.

N_2 adsorption-desorption isotherms were obtained at the N_2 boiling point temperature using Tristar II Kr 3020 Micromeritics equipment. The samples were previously degassed at 120 °C under vacuum for 12 h. Textural parameters were derived from the adsorption data. The specific surface area was determined by Brunauer, Emmett, and Teller (BET) [50] multipoint technique. The pore size distribution was obtained using Density Functional Theory (DFT) and Barret, Joyner, and Halenda (BJH) [50]. The samples were metalized with gold, and their morphology was evaluated by SEM (Zeiss EVO30) using 20 KV. Structural characterization was conducted using XRD and Raman spectroscopy. XRD diffractogram was collected using a GE Seifert Charon XRD, operating at 30 kV and 50 mA using Cr Kα. Diffratograms were obtained between 35° and 166° with 0,01° step. Raman spectra were acquired using a Renishaw inVia Spectrometer System, a laser with 532 nm wavelength at 10% power was focused at the sample through a 20x objective. The integration time was 20 s. Spectra were collected between 100 cm^{-1} and 3200 $cm^{-1,}$ and they were deconvoluted in the range of 800 cm^{-1} and 2000 cm^{-1}, using Lorentzian fit, as indicated by Robertson *et al.* [51].

2.5. SPE procedures.

The RH-AC/Biochar:K_2CO_3 1:3 (800 °C) activated carbon was packed in an empty cartridge with a polypropylene frit at the bottom of the cartridge. After adding the activated carbon, another polypropylene frit was placed on top to compact the particles. Then, the cartridge was set on an SPE manifold device. The SPE cartridge was conditioned with 5 mL methanol and 5 mL water. Then, 1 mL of aqueous phase sample (pH 2.5) was percolated through the cartridge at room temperature under vacuum. The final manometric pressure drop across the cartridge was less than 0.4 bar. After loading, the cartridge was vacuum dried. Residual water was collected in a flask for analysis. The targeted analytes retained on the cartridge were eluted with 5 mL methanol under vacuum. The cartridge was vacuum dried for 2 min. The extract was collected in a 5 mL glass flask and analyzed by HPLC.

2.6. HPLC-DAD analysis.

All HPLC experiments were carried out using a C18 Phenomenex® column (250 mm × 4.6 mm, particle size 4 µm; Kinetex, USA). HPLC-DAD analysis was performed on a Shimadzu HPLC system (model 20-AD) consisting of a binary pump equipped with a DGU-20A degasser, a SIL-20A autosampler, and a CTO-20A column oven. Detection was carried out using an SPD-M20A diode-array detector, which was operated at 280 nm with a resolution of 1 nm. The injection volume was 10 µL. The eluents were water (A) and methanol (B). The mobile phase flow rate was 0.8 mL min^{-1}, and the column oven temperature was 30 °C. The following gradient was used for all experiments: 0–5 min at 5% (B); 5–40 min from 5% to 35% (B); 35–55 min from 35% to 70% (B); 50–55 min, 70% (B); 55–60 min from 70% to 5% (B). Data were acquired and processed with Shimadzu *LC-solution software version 1.25* (Shimadzu Corporation, Japan).

2.7. Method validation.

A standard solution mix of Hydroquinone, 5-hydroxy-methyl-furfural (HMF), Guaiacol, 3-methyl-1,2-cyclopentanodione, 2,6-dimethoxyphenol (syringol), 5-methylfurfural, Homovanillyl alcohol, 4-Hydroxybenzaldehyde, Furfural and Phenol, Resorcinol was prepared in methanol. Standard calibration solutions (1-250 mg mL^{-1}) for assessing linearity were prepared from this stock solution using the mobile phase and injected into the HPLC system. The peak area versus concentration data was treated using linear least squares regression. The analytical parameters that were validated were: specificity, precision, linearity, detection, and quantification limits.

The method specificity was ascertained by analyzing the standard solution mix and samples. The bands for the standards were confirmed by comparing the retention time values and spectra of the band with the standard. The peak purity was assessed by comparing the spectra at three different levels, i.e., at peak start, peak apex, and peak end positions of the spectrum. For the precision test, the intraday (repeatability) and interday (reproducibility) variations for the standard solution mix were performed at the midpoint of the standard curve.

The linearity range of each compound was determined by evaluating the regression curves using a standard external method. The degrees of linearity was expressed by the determination coefficient (R^2) [52]. The limits of quantification and limits of detection were determined using Equations 2 and 3, respectively:

$$\text{Equation 2:} \quad LOQ = 10\,\sigma/S$$

$$\text{Equation 3:} \quad LOD = 3.3\,\sigma/S$$

Where, σ is the standard deviation of the intercept of the calibration plot, and S is the slope of the calibration curve [53].

3. Results and Discussion

3.1. Pyrolysis yield.

The yield of the biochar, according to Equation 1, corresponds to 50.94%. Biochar showed a considerable yield at this temperature compared to other temperatures tested under the same pyrolysis conditions as at 480 °C (Table 1).

Table 1. Biochar performance at different temperatures tested under the same pyrolysis conditions as at 480 °C.

Pyrolysis temperature (ºC)	Biochar yield (%)
410	43.74
480	**50.94**
550	39.2
620	35.26

3.2. Characteristics of activated carbon.

3.2.1 BET, BJH, and DFT.

The nitrogen adsorption-desorption isotherms of activated RH-Biochar varying the amount of activating agent are presented in Figure 1. The profile of isotherm curves is the type I, characteristic of a microporous material, *i.e.*, pores with diameters lower than 2 nm [50]. The surface areas and pore volumes are shown in Table 2. As can be seen, the activation with K_2CO_3 at 800 ºC was very effective in improving the textural characteristics of RH-Biochar, regarding that the increase in the amount of activating agent produces an increase in the surface area, as well as in the pore volume. The isotherm profile remains the same after calcination at 900º C (Figure 1e), allied with a decrease in surface area and pore volume (Table 2).

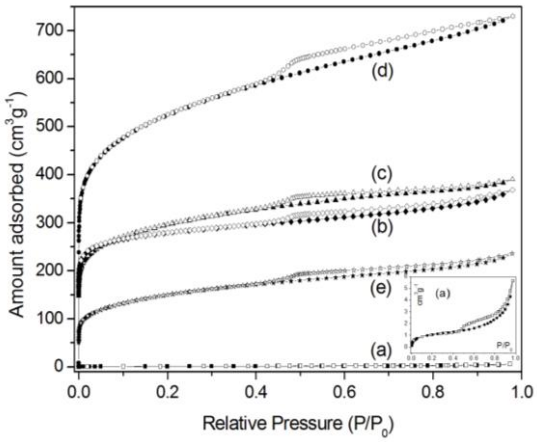

Figure 1. N_2 adsorption-desorption isotherms RH-AC sample series calcinated at 800 ºC. (a) RH-Biochar without calcination; (b) RH-AC/1:1; (c) RH-AC/1:2; (d) RH-AC/1:3; (e) RH-AC/1:3 calcinated at 900 ºC.

Table 2. Textural data.

Material	BET surface area ($m^2 g^{-1}$)	BJH pore volume ($cm^3 g^{-1}$)
RH-Biochar	3.8 ± 0.3	0.008 ± 0.002
RH-AC/1:1/800	997 ± 10	0.27 ± 0.01
RH-AC/1:2/800	1045 ± 10	0.48 ± 0.01
RH-AC/1:3/800	1850 ± 20	0.79 ± 0.01
RH-AC/1:3/900	500 ± 8	0.27 ± 0.01

It is important to highlight that the obtained surface area value for RH-AC/1:3/800 was 1850 $m^2 g^{-1}$. As far as we know, there are no previous reports showing such high surface area for this kind of material, making this system very suitable and promising to be applied as an adsorbent for SPE.

3.3. Morphological and structural characterization.

SEM images of biochar were presented in Figure 2; morphology was heterogeneous with particles ranging a few micrometers to agglomerates higher than 100 µm. In Figure 2 can be observed a detail of one particle, where higher porosity is showed. Some lamellar structure was also observed in this image. The larger surface porosities were not very deep; however,

they are formed by several small porous, as could be seen in figures 2 and 3. These microporous could help in the adsorbing characteristics of this material and corroborates with the BET results.

XRD spectrum shows no peak in the range evaluated, evidencing the amorphous characteristic of the biochar. Raman spectra (Figure 4) showed two well-defined broad bands centered at 1347 cm^{-1} and 1585 cm^{-1}; these bands are assigned as the D and G bands, respectively. Typically, the G band is characteristic of the stretching vibration mode of any pair of sp^2 sites, whether in C=C chains or aromatic rings. Otherwise, the D band is associated with the breathing mode of sp^2 sites in aromatic rings, but not in chains [54].

It is possible to associate the extension of crystallinity with the integrated intensity ratio of D and G bands using the following equation proposed by Cançado *et al.* [55]:

$$\text{Equation 4:} \quad L_a = 2.4 \times 10^{-10} \times \lambda_l^4 \left(\frac{l_D}{l_G}\right)^{-1}$$

where, L_a is the crystallite size in nm, l_l is the wavelength of the laser source, and I_D and I_G are the integrated intensity of D and G Raman bands.

The found crystallite size was 7.5 ± 1.7 nm, showing a small number of crystalline portions in the biochar, in good agreement with DRX results.

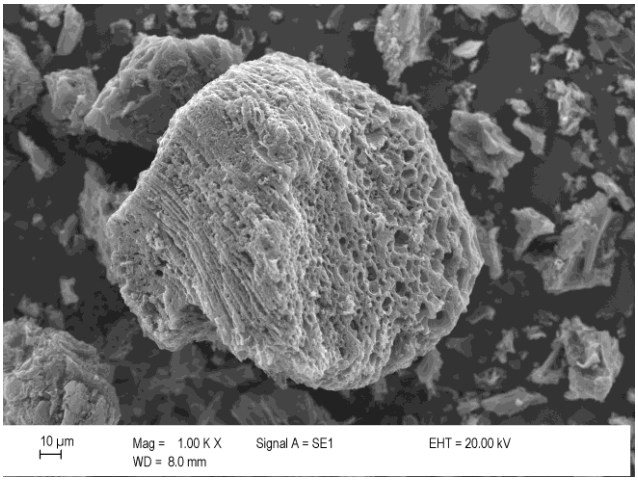

Figure 2. Micrography of the activated charcoal of the rice husk obtained by scanning electron microscopy with a magnification of 1000 x.

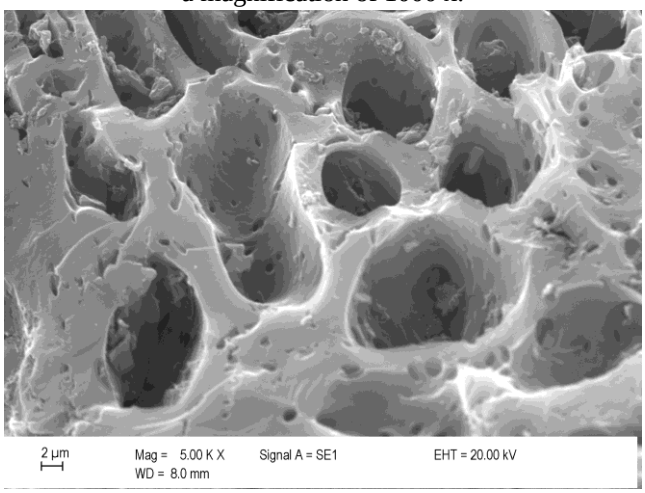

Figure 3. Micrography of the activated charcoal of rice husk obtained by scanning electron microscopy with a magnification of 5000×.

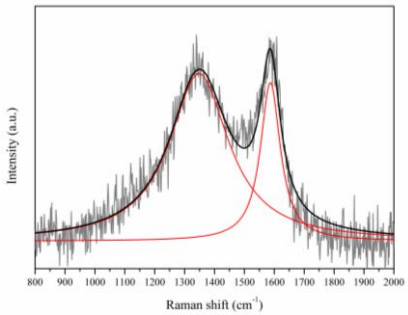

Figure 4. Raman spectrum of activated carbon.

3.3. HPLC-DAD qualitative and quantitative analysis.

Figure 5 (a) shows the HPLC-DAD chromatogram of the aqueous phase (AP) derived from the rice husk bio-oil (examined at 280 nm, which is suitable for these chemicals). Eleven major compounds were identified that are listed in Table 3. All identified compounds were confirmed by comparing their retention time and spectra with standards. These compounds were then quantified using a standard external method.

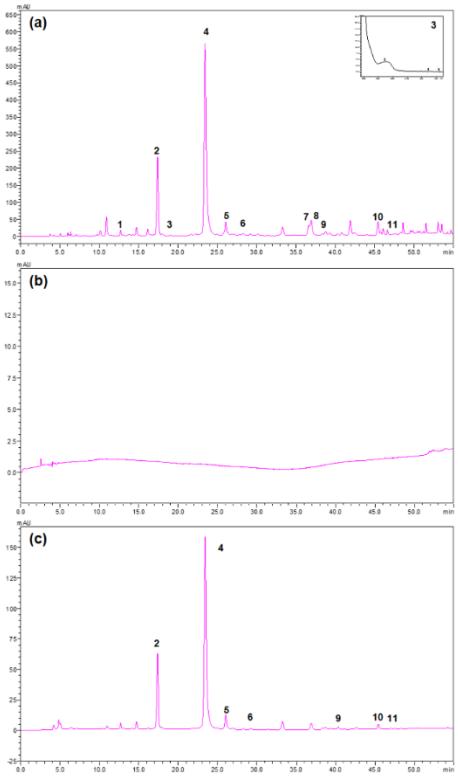

Figure 5. (a) Chromatogram at 280 nm for the aqueous phase, with the absorption spectrum for resorcinol presented in the upper right corner; (b) aqueous phase chromatogram after SPE; (c) chromatogram of methanol extract after compounds removal.

Table 3. Compounds identified in the aqueous phase of rice husk pyrolysis.

Identified Compounds	Peak number
Hydroquinone	1
5-hydroxy-methyl-furfural (HMF)	2
Guaiacol	10
3-methyl-1,2-cyclopentadienone	5
2,6-dimethoxyphenol	11
5-methylfurfural	8
Homovanyl alcohol	6
Phenol	9
4-Hydroxybenzaldehyde	7
Furfural	4
Resorcinol	3

The compounds identified in the rice husk aqueous phase were mainly phenols, furans, and ketones. The rice husk aqueous phase had a composition similar to those reported by Tomasini *et al.* [56] for coconut fibers, sugarcane straw, and sugarcane bagasse. Furaldehydes and ketones were primarily produced from cellulose and hemicellulose by high-temperature pyrolysis, while phenols were mainly produced from lignin [57,58].

Table 4 shows the results of the parametric analyses (linearity, precision, LOD, and LOQ) used in the method validation and the concentration of the identified compounds (averages of three analyses are presented). The calibration curves showed good linearity, as indicated by the correlation coefficients (R^2) for the range of concentrations studied. The R^2 values ranged from 0.996-0.999 for all 11 compounds. The intraday and interday precision tests (expressed in terms of RSD %) showed values below 6.12% for all compounds. These low RSD % values suggested that the developed HPLC-DAD method had good precision. The LOD values ranged from 0.006 for hydroquinone to 0.97 for 5-methylfurfural, whereas the LOQ values ranged from 0.02 to 2.96 for the same compounds. The method specificity was also evaluated. The results indicated that the identified peaks were spectrally homogenous, i.e., there were no coeluting peaks.

Table 4. Validation of analytical parameters and concentration of the compounds identified.

Compounds	Validation range ($mg.L^{-1}$)[a]	Correlation coeficiente	LOD ($mg.L^{-1}$)	LOQ ($mg.L^{-1}$)	Interday precision RSD (%)[b] n=6	Intraday Precision RSD (%)[c] n=6	Concentration ($mg.L^{-1}$) ± SD
Hydroquinone	10-250	0.998	0.006	0.02	5.32	5.25	480.10 ± 0.02
5-hydroxy-methyl-furfural	1-150	0.999	0.17	0.53	5.39	5.02	1082.92 ± 2.73
Guaiacol	1-150	0.999	0.022	0.068	5.17	3.18	1932.46 ± 0.44
3-methyl-1,2-cyclopentadienone	10-250	0.999	0.89	2.71	5.45	3.24	1360.64 ± 0.16
2,6-dimethoxyphenol	1-60	0.998	0.31	0.95	6.10	5.10	338.98 ± 0.14
5-methylfurfural	5-75	0.998	0.97	2.96	4.92	3.56	398.20 ± 0.11
Homovanillyl alcohol	1-100	0.998	0.21	0.65	5.03	3.09	238.26 ± 0.08
Phenol	5-150	0.999	0.23	0.71	5.28	5.07	768.36 ± 0.10
4-Hydroxybenzaldehyde	1-30	0.998	0.10	0.32	4.60	5.61	214.22 ± 0.04
Furfural	1-100	0.998	0.19	0.58	0.09	0.44	3520.87 ± 0.73
Resorcinol	1-250	0.999	0.46	1.39	5.51	3.00	97.42 ± 0.02
2,6-dimethoxyphenol	1-60	0.998	0.31	0.95	6.10	5.10	338.98 ± 0.14
5-methylfurfural	5-75	0.998	0.97	2.96	4.92	3.56	398.20 ± 0.11
Homovanillyl alcohol	1-100	0.998	0.21	0.65	5.03	3.09	238.26 ± 0.08

a) Calibration curves were done at least six concentration levels.
b) Relative standard deviation of assay realized on the same day of a standard mixture, which was injected six times.
c) Relative standard deviation of assay realized on three different days of a standard mixture which was injected six times

To the best of our knowledge, no studies quantified the rice husk aqueous phase by HPLC-DAD. Based on the system validation (precision, linearity, LOD, LOQ, and specificity), the developed method could be successfully employed for the quantification of aqueous phase compounds from bio-oils.

Regarding the chemical composition (Table 4), furfural was the major compound (3520 mg mL^{-1}), followed by guaiacol (1932 mg mL^{-1}), 3-methyl-1,2-cyclopentadienone (1360 mg mL^{-1}) and 5-hydroxy-methyl-furfural (HMF) (1082 mg mL^{-1}). Other identified compounds were present at concentrations between 97 and 768 mg mL^{-1}. Furthermore, higher concentrations of furaldehydes were observed in the rice husk aqueous phase than in the organic phase, which had a predominantly phenolic composition, as was reported by Moraes *et al.* [59]. These authors described the characterization of the organic phase from the pyrolysis of rice husk and reported that phenols accounted for more than 37% (area percentage) of the compounds and aldehydes less than 5%. High value-added chemicals, such as furfural, HMF

and 5-methylfurfural, with high concentrations in the aqueous phase, could serve as a viable alternative feedstock if properly isolated. For example, furaldehydes have been used as lubricants, adhesives, plastics, and nylons, while phenols have been used as disinfectants, resins, and pesticides [60–62].

3.4. Bio-char applied to SPE to remove compounds of the aqueous phase from bio-oil.

After the HPLC-DAD validation, the SPE extraction recovery was calculated to evaluate the efficiency of RH-AC/1:3/800 in removing compounds from the aqueous phase. Figure 5 (b) shows a chromatogram of the aqueous phase sample after the SPE procedure. The majority of compounds were retained in the bio-char solid phase of the SPE cartridge. After their retention on the solid phase, the compounds were extracted with methanol. The resultant chromatogram is shown in Figure 5 (c). Compounds not identified in chromatogram had concentrations lower than the LOQs or were not detected in the extracts.

The percent recoveries of the compounds were calculated based on their initial concentrations in the aqueous phase (using calibration curves) and were between 44.43% to 110%. The percent recovery values were close to 100%, indicating that the analytical method performed well. As can be noted, the efficiency of the RH-AC/1:3/800 stationary phase significantly differed among various compounds. While some analytes showed excellent recoveries, other compounds displayed very strong interactions with the stationary phase. These compounds could not be efficiently extracted. This demonstrated that the activated carbon RH-AC/1:3/800 was efficient for absorbing different, environmentally harmful compounds present in wastewater pyrolysis, which would otherwise have to be recovered before disposal. Adsorption-based technologies, particularly those using activated carbon, have been widely applied in pollution mitigation, e.g., the decontamination of flue gasses and wastewater treatment [63–67]. In wastewater treatment, the efficient removal of organic compounds by activated carbon with K_2CO_3 has been demonstrated in a few studies [21–24].

4. Conclusions

Rice husk biomass can be pyrolyzed to obtain good yields of solid product (biochar). The chemical activation of biochar results in a microporous material with exceptional surface area (1850 m^2g^{-1}). The obtained material was used as an adsorbent to remove the main constituents of the aqueous pyrolysis phase. To evaluate the procedure performed, an HPLC-DAD method was developed and validated. The results showed that furfural was the major compound (3520 mg mL^{-1}), followed by guaiacol (1932 mg mL^{-1}), 3-methyl-1,2-cyclopentadienone (1360 mg mL^{-1}), and 5-hydroxy-methyl-furfural (HMF) (1082 mg mL^{-1}). The SPE process using the activated biochar showed excellent adsorption for the aqueous phase compounds of the rice husk pyrolysis.

The present study suggests that rice husk activated carbon has great potential as a low-cost adsorbent to minimizing the environmental impact caused by organic compounds in the aqueous pyrolysis phase.

Funding

This work was supported by grants from Brazilian Coordenação de Aperfeiçoamento de Pessoal de Nível Superior (CAPES, scholarships for the first author), Finance Code 001.

Acknowledgment

This research has no acknowledgment.

Conflicts of Interest

The authors declare no conflict of interest.

References

1. Natarajan, E.; Sundaram, E.G. Pyrolysis of Rice Husk in a Fixed Bed Reactor. *World Acad. Sci. Eng. Technol.* **2009**, *56*, 504–508, https://doi.org/10.5281/zenodo.1329272.
2. Bakari, R.; Kivevele, T.; Huang, X.; Jande, Y.A.C. Simulation and optimisation of the pyrolysis of rice husk: Preliminary assessment for gasification applications. *J. Anal. Appl. Pyrolysis* **2020**, *150*, 104891, https://doi.org/10.1016/j.jaap.2020.104891.
3. Maciel, G.P. da S.; Machado, M.E.; Barbará, J.A.; Molin, D.D.; Caramão, E.B.; Jacques, R.A. GC × GC/TOFMS analysis concerning the identification of organic compounds extracted from the aqueous phase of sugarcane straw fast pyrolysis oil. *Biomass and Bioenergy* **2016**, *85*, 198–206, https://doi.org/10.1016/j.biombioe.2015.11.009.
4. Opia, A.C.; Hamid, M.K.B.A.; Syahrullail, S.; Rahim, A.B.A.; Johnson, C.A.N. Biomass as a potential source of sustainable fuel, chemical and tribological materials – Overview. *Mater. Today Proc.* **2020**, https://doi.org/10.1016/j.matpr.2020.04.045.
5. Primaz, C.T.; Schena, T.; Lazzari, E.; Caramão, E.B.; Jacques, R.A. Influence of the temperature in the yield and composition of the bio-oil from the pyrolysis of spent coffee grounds: Characterization by comprehensive two dimensional gas chromatography. *Fuel* **2018**, *232*, 572–580, https://doi.org/10.1016/j.fuel.2018.05.097.
6. Hameed, S.; Sharma, A.; Pareek, V.; Wu, H.; Yu, Y. A review on biomass pyrolysis models: Kinetic, network and mechanistic models. *Biomass and Bioenergy* **2019**, *123*, 104–122, https://doi.org/10.1016/j.biombioe.2019.02.008.
7. Zabaniotou, A.; Ioannidou, O. Evaluation of utilization of corn stalks for energy and carbon material production by using rapid pyrolysis at high temperature. *Fuel* **2008**, *87*, 834–843, https://doi.org/10.1016/j.fuel.2007.06.003.
8. Ye, Z.; Liu, L.; Tan, Z.; Zhang, L.; Huang, Q. Effects of pyrolysis conditions on migration and distribution of biochar nitrogen in the soil-plant-atmosphere system. *Sci. Total Environ.* **2020**, *723*, 138006, https://doi.org/10.1016/j.scitotenv.2020.138006.
9. Liu, D.; Zhang, W.; Huang, W. Effect of removing silica in rice husk for the preparation of activated carbon for supercapacitor applications. *Chinese Chem. Lett.* **2019**, *30*, 1315–1319, https://doi.org/10.1016/j.cclet.2019.02.031.
10. Food and Agriculture Organization of the United Nations Statistics Division – FAOSTAT Food and Agricultural commodities production Available online: http://faostat3.fao.org/browse/Q/QC/E.
11. Ministério da Agricultura (MAPA) Perspectivas agropecuaria Available online: http://www.conab.gov.br/OlalaCMS/uploads/arquivos/15_09_24_11_44_50_perspectivas_agropecuaria_2015-16_-_produtos_verao.pdf.
12. Lim, J.S.; Abdul Manan, Z.; Wan Alwi, S.R.; Hashim, H. A review on utilisation of biomass from rice industry as a source of renewable energy. *Renew. Sustain. Energy Rev.* **2012**, *16*, 3084–3094, https://doi.org/10.1016/j.rser.2012.02.051.
13. Hu, L.; He, Z.; Zhang, S. Sustainable use of rice husk ash in cement-based materials: Environmental evaluation and performance improvement. *J. Clean. Prod.* **2020**, *264*, 121744, https://doi.org/10.1016/j.jclepro.2020.121744.
14. Maiti, S.; Dey, S.; Purakayastha, S.; Ghosh, B. Physical and thermochemical characterization of rice husk char as a potential biomass energy source. *Bioresour. Technol.* **2006**, *97*, 2065–2070, https://doi.org/10.1016/j.biortech.2005.10.005.
15. Lu, Q.; Li, W.-Z.; Zhu, X.-F. Overview of fuel properties of biomass fast pyrolysis oils. *Energy Convers. Manag.* **2009**, *50*, 1376–1383, https://doi.org/10.1016/j.enconman.2009.01.001.
16. Singh, P.; Singh, R.K.; Gokul, P. V.; Hasan, S.-U.; Sawarkar, A.N. Thermal degradation and pyrolysis

kinetics of two Indian rice husk varieties using thermogravimetric analysis. *Energy Sources, Part A Recover. Util. Environ. Eff.* **2020**, 1–12, https://doi.org/10.1080/15567036.2020.1736215.
17. Vitasari, C.R.; Meindersma, G.W.; de Haan, A.B. Water extraction of pyrolysis oil: The first step for the recovery of renewable chemicals. *Bioresour. Technol.* **2011**, *102*, 7204–7210, https://doi.org/10.1016/j.biortech.2011.04.079.
18. Rodríguez, I.; Llompart, M..; Cela, R. Solid-phase extraction of phenols. *J. Chromatogr. A* **2000**, *885*, 291–304, https://doi.org/10.1016/S0021-9673(00)00116-3.
19. Fontanals, N.; Marcé, R.M.; Borrull, F. New hydrophilic materials for solid-phase extraction. *TrAC Trends Anal. Chem.* **2005**, *24*, 394–406, https://doi.org/10.1016/j.trac.2005.01.012.
20. Nováková, L.; Vlčková, H. A review of current trends and advances in modern bio-analytical methods: Chromatography and sample preparation. *Anal. Chim. Acta* **2009**, *656*, 8–35, https://doi.org/10.1016/j.aca.2009.10.004.
21. Li, W.; Zhang, L.; Peng, J.; Li, N.; Zhu, X. Preparation of high surface area activated carbons from tobacco stems with K2CO3 activation using microwave radiation. *Ind. Crops Prod.* **2008**, *27*, 341–347, https://doi.org/10.1016/j.indcrop.2007.11.011.
22. Mestre, A.S.; Bexiga, A.S.; Proença, M.; Andrade, M.; Pinto, M.L.; Matos, I.; Fonseca, I.M.; Carvalho, A.P. Activated carbons from sisal waste by chemical activation with K2CO3: Kinetics of paracetamol and ibuprofen removal from aqueous solution. *Bioresour. Technol.* **2011**, *102*, 8253–8260, https://doi.org/10.1016/j.biortech.2011.06.024.
23. Li, M.; Xiao, R. Preparation of a dual Pore Structure Activated Carbon from Rice Husk Char as an Adsorbent for CO2 Capture. *Fuel Process. Technol.* **2019**, *186*, 35–39, https://doi.org/10.1016/j.fuproc.2018.12.015.
24. Zhang, S.; Zhu, S.; Zhang, H.; Liu, X.; Xiong, Y. Synthesis and characterization of rice husk-based magnetic porous carbon by pyrolysis of pretreated rice husk with FeCl3 and ZnCl2. *J. Anal. Appl. Pyrolysis* **2020**, *147*, 104806, https://doi.org/10.1016/j.jaap.2020.104806.
25. Lee, J.-H.; Heo, Y.-J.; Park, S.-J. Effect of silica removal and steam activation on extra-porous activated carbons from rice husks for methane storage. *Int. J. Hydrogen Energy* **2018**, *43*, 22377–22384, https://doi.org/10.1016/j.ijhydene.2018.10.039.
26. Mailler, R.; Gasperi, J.; Coquet, Y.; Derome, C.; Buleté, A.; Vulliet, E.; Bressy, A.; Varrault, G.; Chebbo, G.; Rocher, V. Removal of emerging micropollutants from wastewater by activated carbon adsorption: Experimental study of different activated carbons and factors influencing the adsorption of micropollutants in wastewater. *J. Environ. Chem. Eng.* **2016**, *4*, 1102–1109, https://doi.org/10.1016/j.jece.2016.01.018.
27. Lladó, J.; Gil, R.R.; Lao-Luque, C.; Solé-Sardans, M.; Fuente, E.; Ruiz, B. Highly microporous activated carbons derived from biocollagenic wastes of the leather industry as adsorbents of aromatic organic pollutants in water. *J. Environ. Chem. Eng.* **2017**, *5*, 2090–2100, https://doi.org/10.1016/j.jece.2017.04.018.
28. An, D.; Guo, Y.; Zou, B.; Zhu, Y.; Wang, Z. A study on the consecutive preparation of silica powders and active carbon from rice husk ash. *Biomass and Bioenergy* **2011**, *35*, 1227–1234, https://doi.org/10.1016/j.biombioe.2010.12.014.
29. Guo, Y.; Yang, S.; Yu, K.; Zhao, J.; Wang, Z.; Xu, H. The preparation and mechanism studies of rice husk based porous carbon. *Mater. Chem. Phys.* **2002**, *74*, 320–323, https://doi.org/10.1016/S0254-0584(01)00473-4.
30. Uzunova, A.S.; Uzunov, I.M.; Vassilev, S. V.; Alexandrova, A.K.; Staykov, S.G.; Angelova, D.B. Preparation of low-ash-content porous carbonaceous material from rice husks. *Bulg. Chem. Commun.* **2010**, *42*, 130–137.
31. Yu, Z.; Meng, X.; Liu, N.; Shi, L. A novel disposal approach of deactivated resin catalyst for methyl tert-butyl ether synthesis: Preparation of low-cost activated carbons with remarkable performance on dibenzothiophene adsorption. *Fuel* **2017**, *207*, 47–55, https://doi.org/10.1016/j.fuel.2017.05.053.
32. Budinova, T.; Ekinci, E.; Yardim, F.; Grimm, A.; Björnbom, E.; Minkova, V.; Goranova, M. Characterization and application of activated carbon produced by H3PO4 and water vapor activation. *Fuel Process. Technol.* **2006**, *87*, 899–905, https://doi.org/10.1016/j.fuproc.2006.06.005.
33. Li, X.; Zuo, Y.; Zhang, Y.; Fu, Y.; Guo, Q. In situ preparation of K2CO3 supported Kraft lignin activated carbon as solid base catalyst for biodiesel production. *Fuel* **2013**, *113*, 435–442, https://doi.org/10.1016/j.fuel.2013.06.008.
34. Satayeva, A.R.; Howell, C.A.; Korobeinyk, A. V.; Jandosov, J.; Inglezakis, V.J.; Mansurov, Z.A.; Mikhalovsky, S. V. Investigation of rice husk derived activated carbon for removal of nitrate contamination from water. *Sci. Total Environ.* **2018**, *630*, 1237–1245, https://doi.org/10.1016/j.scitotenv.2018.02.329.

35. Deng, H.; Li, G.; Yang, H.; Tang, J.; Tang, J. Preparation of activated carbons from cotton stalk by microwave assisted KOH and K2CO3 activation. *Chem. Eng. J.* **2010**, *163*, 373–381, https://doi.org/10.1016/j.cej.2010.08.019.
36. Mestre, A.S.; Pires, J.; Nogueira, J.M.F.; Parra, J.B.; Carvalho, A.P.; Ania, C.O. Waste-derived activated carbons for removal of ibuprofen from solution: Role of surface chemistry and pore structure. *Bioresour. Technol.* **2009**, *100*, 1720–1726, https://doi.org/10.1016/j.biortech.2008.09.039.
37. Mai, T.-T.; Vu, D.-L.; Huynh, D.-C.; Wu, N.-L.; Le, A.-T. Cost-effective porous carbon materials synthesized by carbonizing rice husk and K2CO3 activation and their application for lithium-sulfur batteries. *J. Sci. Adv. Mater. Devices* **2019**, *4*, 223–229, https://doi.org/10.1016/j.jsamd.2019.04.009.
38. Adinata, D.; Wandaud, W.; Aroua, M. Preparation and characterization of activated carbon from palm shell by chemical activation with K2CO3. *Bioresour. Technol.* **2007**, *98*, 145–149, https://doi.org/10.1016/j.biortech.2005.11.006.
39. Galhetas, M.; Mestre, A.S.; Pinto, M.L.; Gulyurtlu, I.; Lopes, H.; Carvalho, A.P. Chars from gasification of coal and pine activated with K 2 CO 3 : Acetaminophen and caffeine adsorption from aqueous solutions. *J. Colloid Interface Sci.* **2014**, *433*, 94–103, https://doi.org/10.1016/j.jcis.2014.06.043.
40. Foo, K.Y.; Hameed, B.H. Utilization of rice husks as a feedstock for preparation of activated carbon by microwave induced KOH and K2CO3 activation. *Bioresour. Technol.* **2011**, *102*, 9814–9817, https://doi.org/10.1016/j.biortech.2011.07.102.
41. Foo, K.Y.; Hameed, B.H. Microwave-assisted preparation and adsorption performance of activated carbon from biodiesel industry solid reside: Influence of operational parameters. *Bioresour. Technol.* **2012**, *103*, 398–404, https://doi.org/10.1016/j.biortech.2011.09.116.
42. Foo, K.Y.; Hameed, B.H. Preparation, characterization and evaluation of adsorptive properties of orange peel based activated carbon via microwave induced K2CO3 activation. *Bioresour. Technol.* **2012**, *104*, 679–686, https://doi.org/10.1016/j.biortech.2011.10.005.
43. Temova Rakuša, Ž.; Grobin, A.; Roškar, R. A comprehensive approach for the simultaneous analysis of all main water-soluble vitamins in multivitamin preparations by a stability-indicating HPLC-DAD method. *Food Chem.* **2021**, *337*, 127768, https://doi.org/10.1016/j.foodchem.2020.127768.
44. Urnau, L.; Colet, R.; Gayeski, L.; Reato, P.T.; Burkert, J.F. de M.; Klein, T.; Rodrigues, E.; Jacques, R.A.; Steffens, C.; Valduga, E. Fed-batch carotenoid production by Phaffia rhodozyma Y-17268 using agroindustrial substrates. *Biointerface Res. Appl. Chem.* **2020**, *10*, 5348–5354, https://doi.org/10.33263/BRIAC103.348354.
45. Li, B.; Guo, W.; Ramsey, E.D. Determining phenol partition coefficient values in water- and industrial process water-supercritical CO2 systems using direct aqueous SFE apparatus simultaneously interfaced with on-line SFC and on-line HPLC. *J. Supercrit. Fluids* **2019**, *152*, 104558, https://doi.org/10.1016/j.supflu.2019.104558.
46. Rioux, B.; Rouanet, J.; Akil, H.; Besse, S.; Debiton, E.; Bouchon, B.; Degoul, F.; Quintana, M. Determination of eumelanin and pheomelanin in melanomas using solid-phase extraction and high performance liquid chromatography–diode array detection (HPLC-DAD) analysis. *J. Chromatogr. B* **2019**, *1113*, 60–68, https://doi.org/10.1016/j.jchromb.2019.03.010.
47. Lazzari, E.; Polidoro, A. dos S.; Onorevoli, B.; Schena, T.; Silva, A.N.; Scapin, E.; Jacques, R.A.; Caramão, E.B. Production of rice husk bio-oil and comprehensive characterization (qualitative and quantitative) by HPLC/PDA and GC × GC/qMS. *Renew. Energy* **2019**, *135*, 554–565, https://doi.org/10.1016/j.renene.2018.12.053.
48. Lazzari, E.; Arena, K.; Caramão, E.B.; Herrero, M. Quantitative analysis of aqueous phases of bio-oils resulting from pyrolysis of different biomasses by two-dimensional comprehensive liquid chromatography. *J. Chromatogr. A* **2019**, *1602*, 359–367, https://doi.org/10.1016/j.chroma.2019.06.016.
49. González-González, R.M.; Barragán-Mendoza, L.; Peraza-Campos, A.L.; Muñiz-Valencia, R.; Ceballos-Magaña, S.G.; Parra-Delgado, H. Validation of an HPLC-DAD method for the determination of plant phenolics. *Rev. Bras. Farmacogn.* **2019**, *29*, 689–693, https://doi.org/10.1016/j.bjp.2019.06.002.
50. Gregg, S.J.; Sing, K.S.W. *Adsorption, Surface Area and Porosity*; Academic: London, UK, 1982;
51. Robertson, J. Diamond-like amorphous carbon. *Mater. Sci. Eng. R Reports* **2002**, *37*, 129–281, https://doi.org/10.1016/S0927-796X(02)00005-0.
52. ICH - International Conference on Harmonisation of Technical Requirements for Registration of Pharmaceuticals for Human Use *Q2B Validation of Analytical Procedures*; 1996;
53. Pramod, K.; Ilyas, U.; Kamal, Y.; Ahmad, S.; Ansari, S.; Ali, J. Development and validation of RP-HPLC-

PDA method for the quantification of eugenol in developed nanoemulsion gel and nanoparticles. *J. Anal. Sci. Technol.* **2013**, *4*, 16, https://doi.org/10.1186/2093-3371-4-16.
54. Ferrari, A.C.; Robertson, J. Interpretation of Raman spectra of disordered and amorphous carbon. *Phys. Rev. B* **2000**, *61*, 14095–14107, https://doi.org/10.1103/PhysRevB.61.14095.
55. Cançado, L.G.; Takai, K.; Enoki, T.; Endo, M.; Kim, Y.A.; Mizusaki, H.; Jorio, A.; Coelho, L.N.; Magalhães-Paniago, R.; Pimenta, M.A. General equation for the determination of the crystallite size La of nanographite by Raman spectroscopy. *Appl. Phys. Lett.* **2006**, *88*, 163106, https://doi.org/10.1063/1.2196057.
56. Tomasini, D.; Cacciola, F.; Rigano, F.; Sciarrone, D.; Donato, P.; Beccaria, M.; Caramão, E.B.; Dugo, P.; Mondello, L. Complementary Analytical Liquid Chromatography Methods for the Characterization of Aqueous Phase from Pyrolysis of Lignocellulosic Biomasses. *Anal. Chem.* **2014**, *86*, 11255–11262, https://doi.org/10.1021/ac5038957.
57. Kim, J.-S. Production, separation and applications of phenolic-rich bio-oil – A review. *Bioresour. Technol.* **2015**, *178*, 90–98, https://doi.org/10.1016/j.biortech.2014.08.121.
58. Silva, R.V.S.; Casilli, A.; Sampaio, A.L.; Ávila, B.M.F.; Veloso, M.C.C.; Azevedo, D.A.; Romeiro, G.A. The analytical characterization of castor seed cake pyrolysis bio-oils by using comprehensive GC coupled to time of flight mass spectrometry. *J. Anal. Appl. Pyrolysis* **2014**, *106*, 152–159, https://doi.org/10.1016/j.jaap.2014.01.013.
59. Moraes, M.S.A.; Migliorini, M.V.; Damasceno, F.C.; Georges, F.; Almeida, S.; Zini, C.A.; Jacques, R.A.; Caramão, E.B. Qualitative analysis of bio oils of agricultural residues obtained through pyrolysis using comprehensive two dimensional gas chromatography with time-of-flight mass spectrometric detector. *J. Anal. Appl. Pyrolysis* **2012**, *98*, 51–64, https://doi.org/10.1016/j.jaap.2012.05.007.
60. Surmont, R.; Verniest, G.; De Kimpe, N. Short Synthesis of the Seed Germination Inhibitor 3,4,5-Trimethyl-2(5 H)-furanone †. *J. Org. Chem.* **2010**, *75*, 5750–5753, https://doi.org/10.1021/jo1010476.
61. Huang, J. Hydroquinone modified hyper- cross -linked resin to be used as a polymeric adsorbent for adsorption of salicylic acid from aqueous solution. *J. Appl. Polym. Sci.* **2011**, *121*, 3717–3723, https://doi.org/10.1002/app.33673.
62. Li, Q.; Metthew Lam, L.K.; Xun, L. Cupriavidus necator JMP134 rapidly reduces furfural with a Zn-dependent alcohol dehydrogenase. *Biodegradation* **2011**, *22*, 1215–1225, https://doi.org/10.1007/s10532-011-9476-y.
63. Pietrzak, R.; Bandosz, T.J. Activated carbons modified with sewage sludge derived phase and their application in the process of NO2 removal. *Carbon N. Y.* **2007**, *45*, 2537–2546, https://doi.org/10.1016/j.carbon.2007.08.030.
64. Bhatnagar, A.; Sillanpää, M. Utilization of agro-industrial and municipal waste materials as potential adsorbents for water treatment—A review. *Chem. Eng. J.* **2010**, *157*, 277–296, https://doi.org/10.1016/j.cej.2010.01.007.
65. Carvalho, A.P.; Mestre, A.S.; Haro, M.; Ania, C.O. Advanced Methods for the removal of acetaminophen from Water. In *Acetaminophen: Properties, Clinical Uses and Adverse Effects*; Nova Science Publishers Inc., **2012** ISBN 9781619423749.
66. Karanfil, T. Activated carbon adsorption in drinking water treatment. In *Activated Carbon Surfaces in Environmental Remediation*; Academic Press: New York, **2006**; pp. 345–373.
67. Ogungbenro, A.E.; Quang, D. V.; Al-Ali, K.A.; Vega, L.F.; Abu-Zahra, M.R.M. Synthesis and characterization of activated carbon from biomass date seeds for carbon dioxide adsorption. *J. Environ. Chem. Eng.* **2020**, *8*, 104257, https://doi.org/10.1016/j.jece.2020.104257.